9756 *Biochemistry* **2010,** *49,* 9756–9769
DOI: 10.1021/bi101179g

BIOCHEMISTRY
including biophysical chemistry & molecular biology
Article

Recognition of Nucleoplasmin by Its Nuclear Transport Receptor Importin α/β: Insights into a Complete Import Complex[†]

Jorge Falces,[‡,∥] Igor Arregi,[‡,∥] Petr V. Konarev,[§] María A. Urbaneja,[‡] Dmitri I. Svergun,*[,§] Stefka G. Taneva,[‡,⊥] and Sonia Bañuelos*[,‡]

[‡]*Unidad de Biofísica (CSIC/UPV-EHU), Departamento de Bioquímica y Biología Molecular, Universidad del País Vasco, POB 644, 48080 Bilbao, Spain, and* [§]*European Molecular Biology Laboratory, EMBL c/o DESY, Notkestrasse 85, D-22603 Hamburg, Germany* [∥]*These authors contributed equally to this work.* [⊥]*Present address: Institute of Biophysics, Bulgarian Academy of Sciences, Sofia 1113, Bulgaria.*

Received July 25, 2010; Revised Manuscript Received October 6, 2010

ABSTRACT: Nuclear import of the pentameric histone chaperone nucleoplasmin (NP) is mediated by importin α, which recognizes its nuclear localization sequence (NLS), and importin β, which interacts with α and is in charge of the translocation of the NP/α/β complex through the nuclear pore. Herein, we characterize the assembly of a functional transport complex formed by full-length NP with importin α/β. Isothermal titration calorimetry (ITC) was used to analyze the thermodynamics of the interactions of importin α with β, α with NP, and the α/β heterodimer with NP. Our data show that binding of both importin α and α/β to NP is governed by a favorable enthalpic contribution and that NP can accommodate up to five importin molecules per NP pentamer. Phosphomimicking mutations of NP, which render the protein active in histone chaperoning, do not modulate the interaction with importin. Using small-angle X-ray scattering, we model the α/β heterodimer, NP/α, and NP/α/β solution structures, which reveal a glimpse of a complete nuclear import complex with an oligomeric cargo protein. The set of alternative models, equally well fitting the scattering data, yields asymmetric elongated particles that might represent consecutive geometries the complex can adopt when stepping through the nuclear pore.

Eukaryotic cells need a continuous transit of macromolecules between the cytoplasm and the nucleus, which takes place through the nuclear pore complexes (NPCs) of the nuclear envelope (*1*, *2*). Different carrier proteins are in charge of this transport of cargos, either into (import) or out of (export) the nucleus (*2*). The best understood system for targeting proteins to the nucleus is mediated by the heterodimer formed by importin α (also called karyopherin α) and importin β (or karyopherin β) (*3*, *4*). Importin α recognizes a so-called "classical" nuclear localization sequence (NLS)[1] in the cargo protein, which contains one (monopartite) or two (bipartite) clusters of basic amino acids (*5*, *6*). Importin β is responsible for the translocation of the ternary cargo/α/β complex through the NPC, thanks to interactions with certain nucleoporins (*7*). Once the complex reaches the nucleoplasmic side of the nuclear envelope, the interaction of importin β with the small GTPase Ran elicits its dissociation (*8*), releasing the cargo in the nucleus. The directionality of the transport is given by a gradient of RanGTP, which is predominantly in the GTP-bound form inside the nucleus and the GDP-bound form in the cytoplasm (*9*).

Both importin α and importin β are modular proteins built of α-helical repeat motifs (*3*). In the case of importin α, there are 10 such repeats called ARM (armadillo) (*10*), formed by three α-helices each, that adopt a superhelical twist generating an elongated molecule (*11*). They are preceded by an N-terminal segment of 65 amino acids that constitutes the importin β binding (IBB) domain (*12*, *13*). The available three-dimensional (3D) structures of a truncated importin α lacking the IBB domain (ΔIBB−importin α) bound to NLS peptides (*14*−*21*) have revealed the molecular basis of the interaction and explained why importin α recognizes both mono- and bipartite NLS sequences. The NLS binds in an extended conformation, and antiparallel fashion, to one (in the case of monopartite NLS) or two sites (bipartite NLS) in a concave groove formed by ARM motifs 1−4 (major site) and 6−8 (minor site), establishing hydrophobic, polar, and ionic interactions (*14*−*21*). Importin β is composed of 19 tandem HEAT repeats, each made of two α-helices, that like those of importin α fold in a superhelical fashion (*22*−*24*). Their modular architecture confers upon importins a high degree of flexibility (*25*−*27*); in particular, importin β adopts a differently twisted conformation depending on whether it is free in solution (*26*, *27*) or bound to its different ligands: IBB of importin α (*22*), RanGTP (*23*, *28*), or nucleoporin repeats (*24*). In the complex with the IBB domain of importin α, importin β adopts a closed, snail-like conformation wrapped around the IBB, which

[†]This work was supported by Ministerio de Educación y Ciencia (Grants BFU2007-64452 and SAF2004-07722) and the Basque Government (IT-358-07). J.F. and I.A. hold predoctoral fellowships from the University of the Basque Country and from the Ministerio de Educación y Ciencia, respectively. S.G.T. was a visiting professor at the University of the Basque Country. S.B. was supported by a Ramón y Cajal contract. P.V.K. and D.I.S. acknowledge support by HFSP Grant RGP0055/2006-C.

*To whom correspondence should be addressed. D.I.S.: e-mail, svergun@embl-hamburg.de; telephone, +49 4089 902 125; fax, +49 4089 902 149. S.B.: e-mail, sonia.banuelos@ehu.es; telephone, +34 94 601 8050; fax, +34 94 601 3360.

[1]Abbreviations: NP, nucleoplasmin; NP13D, NP mutant with 13 substitutions for Asp; NLS, nuclear localization sequence; CD, circular dichroism; ITC, isothermal titration calorimetry; SAXS, small-angle X-ray scattering; MW, molecular weight.

 Published on Web 10/06/2010

binds in an extended followed by α-helical conformation to HEAT repeats 7−19 (*22*). In the absence of importin β, it is known that the IBB domain, which has resemblance with a NLS, occupies the NLS binding site of importin α (*11*). This intramolecular interaction plays an autoinhibitory role and is thought to be relevant in the dissociation of the cargo protein inside the nucleus (*11*).

A prototypic substrate of the "classical" importin α/β route is nucleoplasmin (NP), a histone chaperone involved in chromatin remodeling processes, such as sperm decondensation at fertilization (*29*−*31*). NP is pentameric, each monomer, 200 amino acids in length, consisting of two domains, namely, core and tail. The core domains form a compact, hyperstable, β-structured, pentameric ring (*32*), whereas the tails are conformationally flexible (*33*). The NLS motifs of NP are located in the five tail domains, spanning residues 155−170, and belong to the bipartite class (*34*). NP is activated through progressive phosphorylation of multiple residues (*35*, *36*) during *Xenopus* egg maturation, so that when the protein exhibits its maximal activity at the egg stage, it is phosphorylated in both the core and tail domains, some of the phospho residues being located proximal to the NLS (*36*).

Several studies have characterized the binding of importins to peptides corresponding to the NLS of NP (*15*, *16*, *37*) and other proteins (*14*, *17*−*21*, *37*−*39*). Similarly, association of importin β with the IBB domain of importin α has been structurally (*22*) and biophysically (*40*) described. Much less information about importin recognition of native, entire cargo proteins is available, however. Recently, 3D structures of importin α bound to the C-terminal domain of the influenza virus polymerase PB2 subunit (*41*) and to the CBC (cap-binding complex) along with a structural model of the importin α/importin β/CBC complex have been published (*42*). A recent study (*43*) has addressed the interaction between importin α and NLS cargos in living cells, measuring an effective affinity in the cellular environment that is lower than available in vitro data.

Whereas most structural and biophysical studies of importin recognition have dealt with peptides or fragments from nuclear proteins, this work provides information about functional and oligomeric complexes made of full-length proteins. We have thermodynamically and structurally characterized the binding of full-length pentameric NP to importin α, ΔIBB−importin α, and importin α/β, as well as the binding of full-length importin α to importin β. Given that nuclear localization of numerous proteins is modulated through their phosphorylation, which either promotes or inhibits import (*44*, *45*), we have compared importin binding to nonphosphorylated NP and a mutant with phosphorylation mimicking mutations (*36*). Our results indicate that formation of the import complex is mainly driven by recognition of the canonical binding motifs (NLS and IBB). The multiplicity of NLS binding sites within NP and the fact that all of them can be occupied would favor its import, which might explain the preferential nuclear localization of NP. Small-angle X-ray scattering (SAXS) was used to structurally characterize the binary and ternary complexes formed, yielding models that reveal the spatial relationships among the three proteins pointing to asymmetrically positioned α/β heterodimers on the tails of the NP pentamer. The structure of the NP/importin complex shows how the flexibility of NP tail domains allows this protein to accommodate five importin α/β heterodimers.

EXPERIMENTAL PROCEDURES

Purification of the Proteins. Importin α (*Xenopus laevis* α1 sequence) and importin β (human) clones in pQE60 and pQE70, respectively, were kind gifts from Dr. Görlich's laboratory. Both His-tagged proteins were overexpressed in *Escherichia coli* BL21-(pREP4) at 18 °C overnight. Truncated importin α (residues 66−517, termed "ΔIBB−importin α" throughout the text) was subcloned in pET30a (Novagen) (BamHI/XhoI sites) with an N-terminal His tag, using as a template the full-length importin α clone, and overexpressed in *E. coli* BL21(DE3) cells overnight at 18 °C. Cells were disrupted by sonication in 20 mM Tris-HCl (pH 8.0), 500 mM NaCl, 20 mM imidazole (in the case of importin α), 20 mM Hepes (pH 7.5), 500 mM NaCl, and 5 mM imidazole (ΔIBB−importin α) or 50 mM Tris-HCl (pH 7.5), 200 mM NaCl, and 10 mM imidazole (importin β); in all cases, the buffers contained additionally 5 mM $MgCl_2$, 0.1 mM TCEP, 1 mg/mL lysozyme, 10% (v/v) glycerol, and a protease inhibitor cocktail. The proteins were purified from the clarified extract by means of Ni-NTA affinity chromatography (HisTrap FF column, GE Healthcare) followed by gel filtration with Superdex 200 (GE Healthcare) in 50 mM Tris-HCl [pH 8.0 (importin α and ΔIBB−importin α) or pH 7.5 (importin β)], 100 mM NaCl, 2 mM DTT, and 10% glycerol, concentrated, and frozen for storage. Nucleoplasmin (*X. laevis* NPM2 sequence), both the wild type and mutant NP13D, was overexpressed in *E. coli* and purified as previously described (*33*, *36*). Protein concentrations were determined with the BCA colorimetric assay (Pierce), checked spectrophotometrically and occasionally by amino acid analysis. NP concentration values through the text refer to the pentamer. The NLS peptide (KRPAATKKAGQAKKKK) was supplied by NeoMPS (Strasbourg, France).

Gel Filtration Chromatography. Mixtures of nucleoplasmin (5 μM) and different amounts of ΔIBB−importin α to give importin:NP molar ratios between 0 and 10 were prepared in 50 mM Tris-HCl (pH 7.5), 100 mM NaCl, 2 mM DTT, and 10% glycerol and incubated at 20 °C for 1 h. In the case of ternary complexes (5 μM NP, 40 μM importin α, and 60 μM importin), the preformed α/β complex was subsequently incubated with NP. Samples (100 μL) were then centrifuged and loaded onto a Superdex 200 10/30 column (GE Healthcare). Runs were performed at 4 °C and a flow rate of 0.5 mL/min. The eluted fractions were analyzed by sodium dodecyl sulfate−polyacrylamide gel electrophoresis (SDS−PAGE). Densitometry of the gel bands was performed with a G-800 scanner and Quantity One (Bio-Rad).

Dynamic Light Scattering (*DLS*). DLS measurements were taken with a Nano-S Zetaseizer (Malvern Instruments), using a red laser (633 nm), at 20 °C, in 50 mM Tris-HCl (pH 7.5), 100 mM NaCl, 2 mM TCEP, and 10% glycerol. The protein concentration was approximately 2 mg/mL [e.g., close to 5 μM NP in the case of the NP/ΔIBB−importin α (1:5) complex].

Circular Dichroism (*CD*). CD spectra were recorded with a Jasco 720 spectropolarimeter, using quartz cuvettes with a path length of 0.02 cm, in 25 mM Tris-HCl (pH 7.5), 50 mM NaCl, and 10% glycerol. Protein concentrations were 4.5 μM for NP and 18 μM for importin α and importin β. Temperature scans were conducted at 60 °C/h.

Isothermal Titration Calorimetry (*ITC*). ITC measurements were taken using a VIP-ITC MicroCalorimeter (MicroCal, Inc., Northampton, MA). Proteins were dialyzed in a buffer containing 50 mM Tris-HCl (pH 7.5), 100 mM NaCl, 2 mM TCEP, and 10% glycerol [we have observed (not shown) that

glycerol addition enhances importin α stability] and degassed prior to the experiment. Measurements were performed at 20 °C, unless indicated. For analysis of importin α/β binding energetics, either importin α or β, at 15 μM, was titrated onto the other importin at 1.2−3 μM; both measurements gave equivalent results. Injections of either 6 or 8 μL were performed at 320 s intervals (the first injection always was of 1 μL and is not considered in data analysis). Interaction of ΔIBB−importin α with NP was analyzed via titration of 80−100 μM ΔIBB−importin α onto approximately 2 μM NP. In the case of the interaction of importin α/β with NP, 28−46 μM heterodimer, with an excess of importin β, was added to the calorimetric cell containing the NP solution at 0.6−1 μM. Titrations were also performed in the reverse mode via addition of NP (19 μM) to importin α/β (3 μM), which gave equivalent parameters. Binding of importin α/β to the NLS peptide was assessed via addition of 26−40 μM peptide to 2−3.2 μM importin α/β. For comparison, the binding of importin α alone or importin β alone to NP was also investigated, using the mentioned concentrations. The corresponding heat of dilution of each protein titrated into buffer was used to correct the data. No change in the oligomeric state of any of the species under study was observed.

The heat of the reaction of each injection is related to the calorimetric enthalpy of binding, $\Delta H°$. The binding isotherms, $\Delta H°$ versus molar ratio, were analyzed with an independent binding sites model using MicroCal Origin. The fit of the binding curve yields the binding constant K_a ($K_d = 1/K_a$) and the enthalpy $\Delta H°$ of the binding reaction. The Gibbs free energy of binding ($\Delta G°$) and the entropy ($\Delta S°$) are determined from the basic thermodynamic expression $\Delta G° = -RT \ln K_a = \Delta H° - T\Delta S°$, where R and T are the gas constant and the absolute temperature, respectively.

Titration experiments were performed at several temperatures in the range from 10 to 20 °C, the rather low thermal stability of importin [and especially ΔIBB−importin α (see below)] precluding measurements at higher temperatures. The change in heat capacity ($\Delta c_P = \partial \Delta H/\partial T$), estimated from the linear fit of $\Delta H°$ versus temperature dependence, provides a measure of the change in the solvation of the proteins and solvent release upon complex formation (*46*). The heat capacity change of binding is used to estimate the changes in the solvation entropy component upon binding

$$\Delta S_{solv} = \Delta c_P \ln(T/T*)$$

where $T*$ (385.15 K) is the temperature of entropy convergence (*47*), and to dissect the observed entropy change of binding into different contributions (*48*)

$$\Delta S = \Delta S_{conf} + \Delta S_{solv} + \Delta S_{tr}$$

where the conformational entropy component ΔS_{conf} is related to changes in the conformational degree of freedom for the side chains and probably for the backbones, the solvation term ΔS_{solv} reflects changes in hydration entropy upon formation of a complex, and ΔS_{tr} reflects changes in translational and rotational degrees of freedom. The translational and rotational entropy is assumed to be close to the cratic entropy [$\Delta S_{tr} = \delta S_{cratic} = R \ln(1/55) = -7.98$ cal mol^{-1} K^{-1}] (*49*).

Small-Angle X-ray Scattering (*SAXS*). Small-angle X-ray scattering patterns of importin α/β, ΔIBB−importin α/NP, and importin α/β/NP complexes were recorded on beamline I711 of the Max-Lab on storage ring MaxLab-II (Lund, Sweden) (*50*) and on beamline X33 EMBL on storage ring DORIS-III (Hamburg, Germany). Saturated complexes were either isolated by gel filtration or prepared in situ by mixing adequate amounts of the proteins. The samples were found to be homogeneous, eluting as isolated peaks, in less than 2 mL from the Superdex 200 10/30 column. Furthermore, the polydispersity index of NP complexes as measured by DLS was below 0.2. The total protein concentration was between 0.25 and 10.0 mg/mL (for comparison with concentrations used in other techniques, 2 mg/mL ternary complex corresponds to 2.2 μM NP), and 5 mM DTT was added to the samples before the measurements to prevent radiation damage. The data were recorded at 15 °C, using a MAR345 two-dimensional image plate detector (I711) or a pixel 1M PILATUS detector (DECTRIS) (×33) at a sample−detector distance of 2.2 or 2.7 m, respectively, and a wavelength (λ) of 0.15 nm, covering the range of momentum transfer 0.12 nm^{-1} < s < 2.5 (5.5) nm^{-1} ($s = 4\pi \sin\theta/\lambda$, where 2θ is the scattering angle). No radiation damage was observed. All data manipulations were performed by using PRIMUS (*51*). The forward scattering $I(0)$ and the radius of gyration R_g were evaluated using the Guinier approximation (*52*) assuming that at very small angles ($s < 1.3/R_g$) the intensity is represented as $I(s) = I(0) \exp[-(sR_g)^2/3]$. These parameters were also computed from the entire scattering patterns using GNOM (*53*), which provides maximum particle dimensions (D_{max}) and pair distance distribution functions [$p(r)$]. The molecular weights (MW_{exp}) of the solutes were estimated from the forward scattering by normalization against reference solutions of bovine serum albumin. The excluded (Porod) volumes of hydrated particles were computed as described in ref *54*:

$$V_p = 2\pi^2 I(0) / \int_0^\infty s^2 I(s)\, ds$$

Prior to the calculation, an appropriate constant was subtracted from each data point to force the s^{-4} decay of the intensity at higher angles following Porod's law (*54*) for homogeneous particles. This procedure yields a "shape scattering" curve corrected for the unwanted scattering contribution from the internal structure.

DAMMIF (*55*), a fast version of DAMMIN (*56*), used to reconstruct the low-resolution shape of importins α/β and their complexes with NP, represents the particle as a collection of $M \gg 1$ densely packed beads inside a sphere with a diameter D_{max}. In DAMMIF, each bead is assigned either to the solvent or to the particle and the latter is represented by a simple "phase" (nonsolvent beads). Starting from a random string, simulated annealing (SA) is employed in DAMMIF to search for a model composed by interconnected compact phases, which fits to the experimental curve to minimize the overall discrepancy:

$$\chi^2 = \frac{1}{N-1} \sum_j \left[\frac{I(s_j) - cI_{calc}(s_j)}{\sigma(s_j)} \right]^2$$

where N is the number of experimental points, c is a scaling factor, and $I_{calc}(s_j)$ and $\sigma(s_j)$ are the calculated intensity and the experimental error at momentum transfer s_j, respectively. The results of multiple DAMMIF runs (20 runs) were averaged to determine common structural features using DAMAVER (*57*) and SUPCOMB (*58*).

Molecular modeling for the NP/importin complexes was conducted using the atomic model of the NP core pentamer [monomer residues 16−118; Protein Data Bank (PDB) entry 1K5J (*32*)] and the crystallographic models of importin α bound

to the NLS peptide from NP [residues 68−489; PDB entry 1EE5 (*15*)] and importin β [residues 1−876 and 44 residues of the IBB domain of importin α; PDB entry 1QGK (*22*)] with SASREF (*59*). To model the structure of the importin α/β/NP complex in solution, we used the restored C-terminal tails of the NP pentamer (monomer residues 119−200) (*60*) as five independent rigid bodies connected to the corresponding NP core pentamer parts. The contact restraints between NP tails and importin α (to have contact distances of ~7−10 Å) were applied to provide interactions between NLS segments of the NP tail (residues 155−170) and the middle part of importin α (residues 180−380) according to Conti et al. (*15*).

An SA protocol implemented in SASREF (*59*) was employed to find an interconnected assembly of subunits without steric clashes fitting the scattering data. The scattering amplitudes of the known high-resolution models were calculated from their atomic coordinates with CRYSOL (*61*), and their positions and orientations were established to fit simultaneously the scattering from importin α/β/NP and ΔIBB−importin α/NP complexes by 5:5:1 and 5:1 assembly, respectively. The rigid body modeling of the ternary and binary complexes was also performed using another homologue structure of importin α (PDB entry 1EJY) (*16*), and similar results were obtained. All the calculations presented here were performed without accounting for the His tags of importin α and β; the modeling was also done with the His tags added as dummy residue chains, and this addition yielded no noticeable effect on the reconstructed models.

The flexibility of the ternary complex was assessed by an ensemble optimization method (EOM) (*62*). Coexisting conformers were selected using a genetic algorithm from a pool containing a large number of randomly generated models. An ensemble pool of 10^5 structures (with and without imposing *P*5 symmetry using the same domains and restraints as for the rigid body modeling) was generated to find the subsets of the conformer models, a mixture of which fitted the experimental data. Multiple runs of EOM (20 independent runs; for each EOM run, the genetic algorithm process was repeated 50 times using the default parameters of the genetic algorithm, i.e., 1000 generations, 50 ensembles of theoretical curves, 20 curves per ensemble, 10 mutations per ensemble, and 20 crossings per generation) were performed and the obtained subsets analyzed to yield the R_g distributions in the optimal ensembles.

OLIGOMER (*51*) was used to calculate the ratio of monomeric and dimeric species present in ΔIBB−importin α solutions at low concentrations (0.25−1 mg/mL). The experimental intensity $I_{exp}(s)$ was represented by linear combinations of the curves computed from the putative dimeric model of ΔIBB−importin α at high concentrations (5−10.0 mg/mL) obtained using SASREF (*59*) and the monomeric part from this model. Given the scattering curves of such components, OLIGOMER finds the volume fractions of each component by solving a system of linear equations to minimize the discrepancy between the experimental and calculated scattering curves.

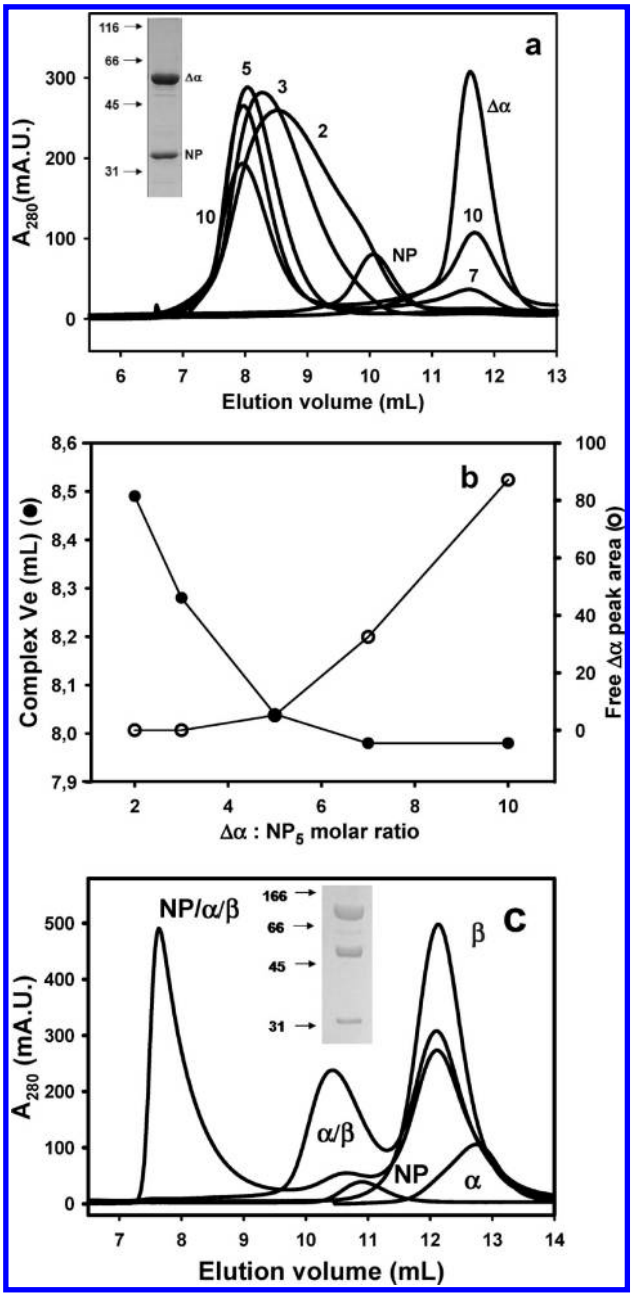

FIGURE 1: Formation of saturated ΔIBB−importin α/NP and α/β/NP complexes. (a) Size exclusion chromatography profiles of ΔIBB−importin α, NP, and importin/NP mixtures at molar ratios of 2, 3, 5, 7, and 10. The mixtures were run in a Superdex 200 column. The inset shows the SDS−PAGE analysis of a fraction corresponding to the saturated complex. (b) Elution volume of the complex (●) and area of the band corresponding to excess importin (○) as a function of importin:NP molar ratio in the initial chromatographic mixtures. (c) Elution profiles of NP/α/β mixtures with a 1:7:10 molar ratio, an α/β mixture with a 1:1.5 molar ratio, and the isolated proteins (NP, importin β, and importin α). The inset shows the SDS−PAGE analysis of an elution fraction corresponding to the saturated complex.

RESULTS

Nucleoplasmin Forms a Stable Complex with Importin α/β. To establish the formation of the complex between full-length NP and importin α or the heterodimer α/β as well as between importin α and β, we used size exclusion chromatography. First, we studied the interaction of NP with ΔIBB−importin α, a truncated form of importin α lacking the autoinhibitory IBB domain (the N-terminal 65 residues), that is able to stably bind NLS-containing proteins. It has been shown (*37*) that the NLS binding properties of ΔIBB−importin α are most similar to those of the importin α/β heterodimer that functions in vivo.

When a mixture of NP and ΔIBB−importin α is injected into a gel filtration column, both proteins coelute at a volume smaller than those of the corresponding isolated proteins (Figure 1a).

The comparison of the elution profiles of mixtures with NP:ΔIBB−importin α molar ratios of up to 1:10 (Figure 1a,b) indicates that upon addition of increasing amounts of importin, the elution volume of the complex decreases, reflecting its bigger size, up to a molar ratio of approximately five importins per NP. The complex size does not increase further at higher ΔIBB−importin α:NP molar ratios, and an excess of free importin starts appearing (Figure 1a,b). This indicates that in the saturated complex all five NLS binding sites within NP are available for the binding of importin, and NP can accommodate five importins simultaneously. Furthermore, the shape of the band corresponding to the saturated complex reflects the fact that it behaves as a homogeneous species. Densitometric analysis of the electrophoresis bands corresponding to these chromatographic fractions (Figure 1a, inset) suggests a stoichiometry of five molecules of ΔIBB−importin α per NP in the saturated complex. One should take into account the fact that the ΔIBB−importin α concentration used in these experiments (40 μM) is well above the K_d as determined by ITC (54 nM; see below), so when an excess of importin is present, all the binding sites of NP can be occupied. Therefore, the results obtained by gel filtration suggest that a homogeneous, saturable complex with a defined composition of five molecules of ΔIBB−importin α per NP pentamer forms.

To form the NP/α/β ternary complex (notice that full-length importin α is used in this case), nucleoplasmin was incubated with an excess of the heterodimer importin α/β (1:8 molar ratio). Previously, and with the aim of avoiding the presence of free importin α, which can also bind NP (see below) and that would hinder the interpretation of the results, importins α and β were mixed in a 1:1.5 molar ratio. The protein concentrations used (40 μM importin α and 60 μM importin β) are well above the K_d of their binding (see below); therefore, virtually all of the importin α should be forming part of the heterodimer. Figure 1c shows the chromatographic elution profile of the NP/α/β ternary mixture along with the profiles of α/β and the three isolated proteins, for comparison. NP, importin α, and importin β coelute in a single peak, as checked by electrophoresis (Figure 1c, inset), at an elution volume that corresponds to a species clearly larger than the NP pentamer and the α/β heterodimer, indicating that a ternary complex is formed. Analysis by densitometry of the relative intensity of the electrophoresis bands (inset) gives an estimation of a molar ratio of approximately 5.5 α/β heterodimers per NP pentamer. This complex seems to be saturated, because an excess of heterodimer α/β and free importin β can be observed (Figure 1c). Because the elution volume of the complex falls close to the resolution range limit of this column, to rule out the possibility of aggregation and/or heterogeneity, the formation of a discrete ternary complex was also confirmed with a Superose 6 column (data not shown).

Energetics of the Formation of the Importin α/β Heterodimer and Importin α/NP Binary and Importin α/β/NP Ternary Complexes. Figure 2 shows the calorimetric profile of a titration of importin α with importin β and the fit of the binding isotherm, reflecting the fact that the formation of the α/β heterodimer is a process driven by exothermic enthalpy. The binding interaction is characterized by 1:1 stoichiometry, as expected (*63*), and an affinity of 153 nM (Figure 2 and Table 1). The latter is similar to previously reported K_d values (*37*, *64*). The dependence of the enthalpy change with temperature is accompanied by a large negative heat capacity change, Δc_P (Table 1), which should arise from changes in the solvation occurring upon binding of importins. This Δc_P value (−840 cal mol^{-1} K^{-1}) is in good agreement with that predicted from the buried polar and apolar solvent accessible areas (ΔASA) [1402.5 and 2426.7 Å^2, respectively, according to the X-ray structure of importin β bound to the IBB domain of importin α (*22*), from which a Δc_P value of −727.4 cal mol^{-1} K^{-1} can be estimated] (*48*), suggesting that importin α contributes to the contact area merely through the IBB domain.

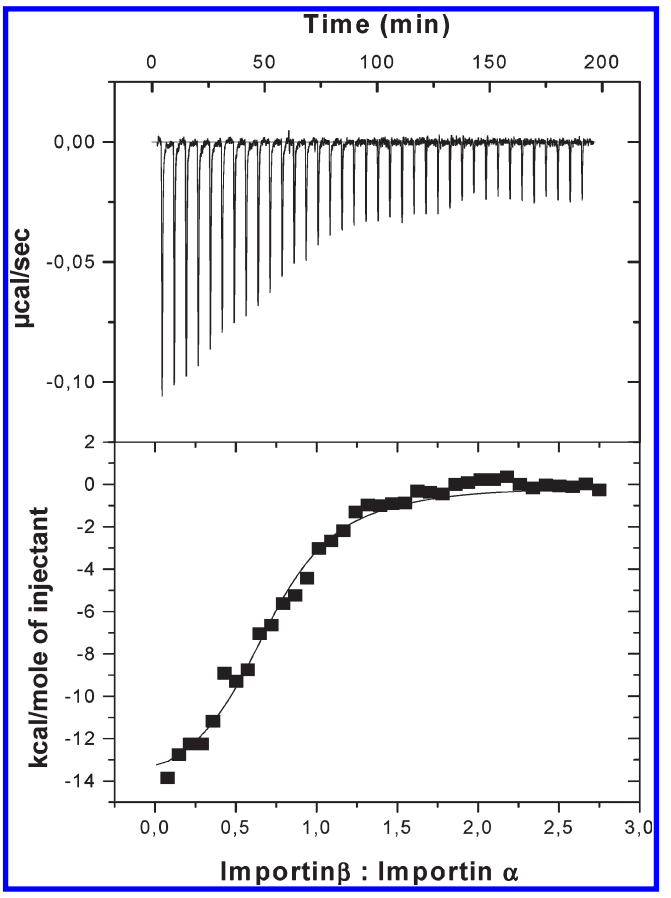

FIGURE 2: Isothermal titration of importin α with importin β. The top panel presents the baseline-corrected instrumental response of successive additions of importin β (15 μM) to importin α (2 μM); the bottom panel shows the integrated data (■) and the fit of the binding isotherm by an independent binding sites model (—).

To describe the energetics of formation of the NP/α/β complex, we conducted both direct, in which α/β was injected on the NP solution, and reverse, for which NP was added to the α/β solution (see Figure 3), titrations, yielding equivalent results. In both cases, the α/β complex was preformed with an excess of importin β to guarantee that no free importin α, which is also able to bind to NP (see below), was present. ITC measurements showed no detectable binding between importin β and NP, as expected (data not shown). The corresponding binding isotherms were well fitted with an independent binding sites model (Figure 3, bottom) that yielded a stoichiometry of five importin α/β heterodimers per NP pentamer (Table 1). Importin α/β exhibits a high-affinity binding interaction with NP, K_d being 57 nM. A large enthalpy change (ΔH° = −29.6 kcal/mol), associated with strong polar interactions, e.g., hydrogen bonding, van der Waals, and/or electrostatic interactions, upon complex formation, is counterbalanced by a large unfavorable entropic contribution to the free energy of binding. The entropic penalty is most likely correlated with the reduced mobility of amino acid residues at the binding interface and/or conformational changes of the proteins upon binding.

Table 1: Summary of the Thermodynamic Data for the Formation of the Complex of Importin α with Importin β, ΔIBB−Importin α with NP and NP13D, Importin α with NP, and Importin α/β with NP and NLS[a]

	α/β	α/β/NLS	α/β/NP	α/NP	Δα/NP	Δα/NP13D
n	0.92 ± 0.08	0.7 ± 0.1	4.9 ± 0.3	5.3 ± 0.1	4.84 ± 0.4	5.0 ± 0.06
K_d (nM)	153 ± 62	116 ± 12	57 ± 15	513 ± 87	54 ± 6	48 ± 6
$\Delta H°$ (kcal/mol)	−12.7 ± 0.9	−29.6 ± 0.5	−29.6 ± 0.8	−9.8 ± 0.5	−18.5 ± 1.8	−20.4 ± 1.8
$-T\Delta S°$ (kcal/mol)	3.6 ± 1.2	20.3 ± 0.4	19.8 ± 0.6	1.37 ± 0.4	8.8 ± 1.6	10.6 ± 1.7
$\Delta G°$ (kcal/mol)	−9.1 ± 0.4	−9.3 ± 0.1	−9.7 ± 0.2	−8.43 ± 0.1	−9.8 ± 0.2	−9.8 ± 0.1
Δc_P (cal mol^{-1} K^{-1})	−840 ± 22	−796 ± 48	−817 ± 71	nd[b]	nd	nd
ΔS_{solv} (cal mol^{-1} K^{-1})	229	217	223			
ΔS_{conf} (cal mol^{-1} K^{-1})	−234	−278	−282			

[a]ITC measurements were performed at 20 °C, in buffer containing 50 mM Tris-HCl (pH 7.5), 100 mM NaCl, 2 mM TCEP, and 10% glycerol. [b]nd = not determined.

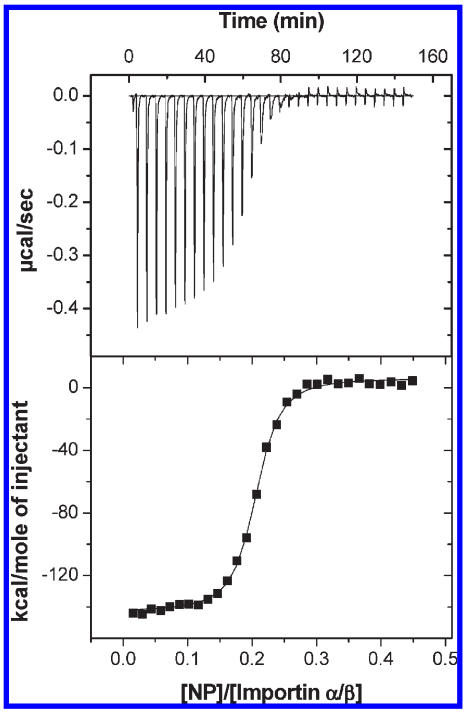

FIGURE 3: Isothermal titration of importin α/β with NP. Titration of NP (50 μM) into importin α/β (1 μM) (top panel) and the fit of the binding isotherm by an independent binding sites model (bottom panel).

We also measured the binding of importin α/β to a peptide corresponding to the NLS sequence (Table 1). It is noteworthy that importin binds similarly to the NLS when the latter is isolated or in the context of the full-length NP macromolecule, suggesting that no other regions of NP significantly contribute to the binding. However the rest of the protein might have a role in modulating the specificity for different importin α subtypes other than importin α1 (*65*). The enthalpy of binding of importin α/β to NP, as well as to the NLS peptide, is strongly temperature dependent (Figure 4), resulting in similar large negative Δc_P values, −817 and −796 cal mol^{-1} K^{-1} for the formation of the complexes of importin α/β with full-length nucleoplasmin and NLS, respectively, which suggests that the surface area buried within the binding interface is comparable in both cases. From the experimental value of Δc_P, the solvation entropy term was estimated and used to decompose the entropic term into different components. In the interaction of importin α/β with NP, there is an entropic penalty associated with the loss of conformational flexibility upon binding (ΔS_{conf} = −282 cal mol^{-1} K^{-1}), probably arising from the "rigidification" of the NLS segment in the otherwise mobile NP tails (*33*). This conformational entropy change is unfavorable and greater than the favorable solvation entropy (ΔS_{solv} = 223 cal mol^{-1} K^{-1}) associated with hydrophobic interactions, thus resulting in an unfavorable entropy contribution to the Gibbs free energy of binding (Table 1).

In the absence of importin β, full-length importin α is able to bind NP, too, albeit with a lower affinity (Table 1), as expected from the autoinhibitory role of the IBB domain (*11*, *66*), and with a lower enthalpic contribution to the free energy of binding (Table 1). The decrease in affinity we observe agrees with what has been described in other studies using the NLS peptide (*8*, *37*). The fact that the enthalpy change associated with the binding of full-length importin α is less favorable than in the case of the α/β heterodimer could be related to the displacement of the IBB domain from the NLS binding site to allow NP binding, whereas this domain is already in an "open" conformation in the case of the α/β heterodimer. Additionally, the entropic contribution is much less unfavorable than in the case of α/β (Table 1), which could reflect, among others, a conformational change associated with the "release" from the NLS binding site of the previously ordered and bound IBB domain, to allow the interaction.

By contrast to full-length importin α, whose binding to NP is inhibited, the truncated ΔIBB−importin α shows a similar affinity for NP than importin α/β (Table 1), in agreement with the described binding properties using NLS peptides (*17*, *37*), with binding enthalpy and entropy values between those of importin α/β and full-length importin α (Table 1).

To explore the possible influence of NP phosphorylation on its recognition by importin α, we have also analyzed the binding of importin to the phosphorylation mimicking mutant NP13D. This mutant contains 13 substitutions of phosphorylatable residues for Asp and acquires the same functional properties as natural hyperactivated egg NP, in contrast to inactive recombinant wild-type NP (*36*). NP13D binds to ΔIBB−importin α with the same stoichiometry, affinity, and favorable enthalpy as wild-type NP (Table 1), suggesting that NP phosphorylation does not affect its interaction with importin.

Altogether, these results show that NP can bind up to five importin α/β heterodimers and suggest that the interaction, which is enthalpically driven, is just mediated by the recognition of the NLS sequence of NP tail domains. The fact that a NP mutant in which the NLS has been invalidated by substitution of Lys residues 167 and 168 with Asn does not bind ΔIBB−importin α (Figure S1 of the Supporting Information) further supports the notion that the rest of NP does not significantly contribute to the interaction.

Stabilization of the Proteins upon Binding. To evaluate the effect of the formation of the complex on the secondary structure

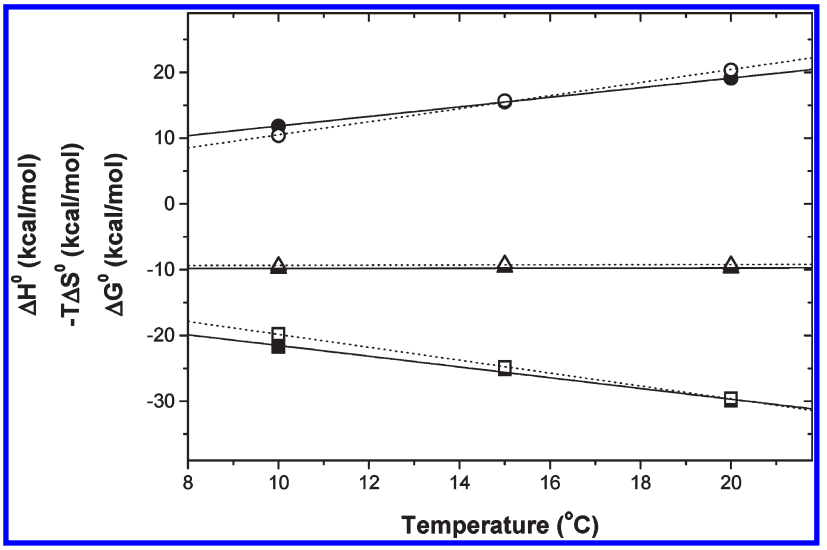

FIGURE 4: Temperature dependence of the thermodynamic parameters of importin α/β binding to NP and NLS. It provides the heat capacity change ($\Delta c_P = \partial \Delta H/\partial T$) for the binding of importin α/β to NP (filled symbols) and NLS (empty symbols): $\Delta H°$ (■ and □), $-T\Delta S°$ (● and ○), and $\Delta G°$ (▲ and Δ). Titrations were performed at 10, 15, and 20 °C.

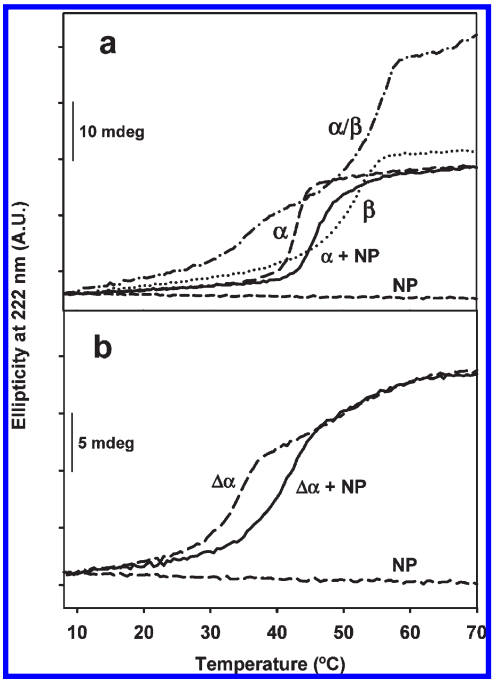

FIGURE 5: Stabilization of importin α upon binding to NP. Thermal denaturation profiles of the different proteins as monitored by circular dichroism, normalized to the same initial ellipticity value. (a) Importin α and complexes thereof and (b) ΔIBB−importin α (Δα) alone and in a complex with NP.

and stability of its constituent proteins, we analyzed NP, importin α, and importin β and different mixtures thereof by circular dichroism (CD) spectroscopy. Importin α (both ΔIBB and full-length forms) and importin β display typical far-UV CD spectra of α-helical proteins, with ellipticity minima at 208 and 222 nm, as expected from their 3D structures (*11*, *22*) (see Figure S2 of the Supporting Information). The spectrum of the importin α/β complex (at a 1:1 molar ratio) does not significantly differ from the sum of their spectra, suggesting that there is no gross change in secondary structure upon association of these proteins (Figure S2 of the Supporting Information). The described (*22*, *40*) folding of part of the IBB domain upon binding to importin β probably has a minor contribution and is not reflected in the total ellipticity of the complex. Following the ellipticity at 222 nm, we monitored their stability toward thermal denaturation (Figure 5). Importin α and β unfolding transitions are characterized by T_m values of 41.5 and 52.2 °C, respectively. A thermal scan of the α/β complex shows two transitions: one most likely corresponding to importin β in a complex with IBB, which is shifted to a slightly higher temperature (T_m = 53.5 °C) with regard to importin β alone, and a new, smaller transition, centered at 35 °C (Figure 5a). The fact that ΔIBB−importin α shows a denaturation T_m of 34.0 °C (see below) suggests that the low-temperature transition of the α/β complex corresponds most probably to importin α, destabilized by the uncovering of its NLS binding site when the IBB domain is engaged in the interaction with β. In the α/β heterodimer, the two proteins show independent transitions; this, together with the fact that the stability of importin β in the heterodimer is similar to that described for its complex with the IBB domain (*40*) and the stability of importin α is as that of isolated truncated importin α, suggests that the two importins are not intimately associated but instead behave as independent units in the heterodimer, probably connected solely by the IBB domain.

The far-UV CD spectrum of NP (Figure S2 of the Supporting Information) indicates a combination of β [corresponding to the core domain (*32*)] and nonregular structures (mainly at the tail domain of the protein) as previously described (*33*). The CD spectrum of the NP/ΔIBB−importin α complex (1:4 molar ratio) (Figure S2 of the Supporting Information) is dominated by the contribution of the helical structure of importin and is not significantly different from that resulting from the addition of the signals of the isolated proteins. This result suggests that complex formation does not involve detectable changes in the secondary structure of either protein, as expected considering that binding to the NLS peptide does not substantially modify the 3D structure of importin α (*14*). The ellipticity value at 222 nm of ΔIBB−importin α shows the already mentioned transition centered at 34.0 °C, and a second, less cooperative, thermal transition centered at approximately 50 °C and observed as a slight gradual loss of ellipticity. The spectrum of the protein at 70 °C is still characteristic of a helical protein ($\theta_{222} = -10000$ deg cm^2 dmol^{-1}) (data not shown), reflecting the presence of residual

Table 2: Overall SAXS Parameters[a]

sample	R_g (nm)	D_{max} (nm)	V_p (nm^3)	MW_{exp} (kDa)	MW_{th} (kDa)	χ_D	χ_S
ΔIBB−importin α	4.32 ± 0.15	16.0 ± 0.5	210 ± 15	110 ± 10	108 (dimer)	1.42	1.82
importin β	3.65 ± 0.10	13.0 ± 0.5	185 ± 15	105 ± 15	98 (monomer)	1.29	1.44
α/β (1:1)	5.70 ± 0.20	19.0 ± 0.8	390 ± 20	185 ± 30	160 (1:1)	1.12	1.19
α/β (2:2)	7.50 ± 0.20	25.0 ± 0.8	650 ± 20	345 ± 30	320 (2:2)	1.13	1.58
NP/ΔIBB−importin α (1:5)	6.35 ± 0.25	20.0 ± 1.0	810 ± 30	410 ± 40	380 (1:5)	1.06	1.29
NP/α/β (1:5:5)	8.57 ± 0.25	28.0 ± 1.0	1800 ± 100	860 ± 50	900 (1:5:5)	1.24	1.87

[a] R_g, radius of gyration; D_{max}, maximum size of the particle; V_p, excluded volume of the hydrated particle estimated from ab initio models (DAMMIN); MW_{exp}, estimated molecular weight; MW_{th}, theoretical molecular weight (for the specified stoichiometries); χ_D and χ_S, values for the fit curves from ab initio models (DAMMIN) and from rigid body modeling using SASREF (for importin β, CRYSOL fit), respectively.

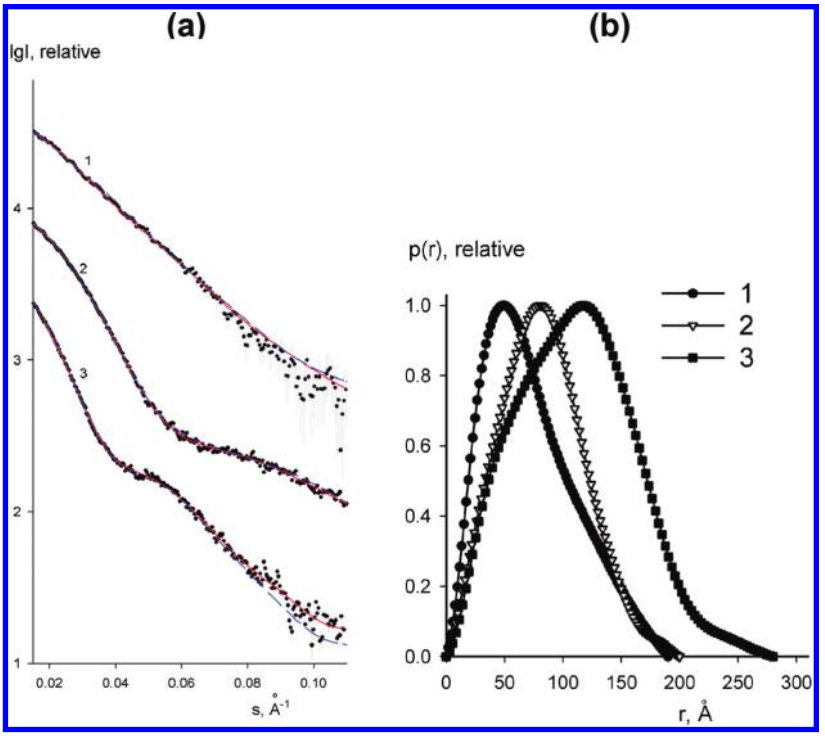

FIGURE 6: Scattering data. (a) Experimental scattering patterns (dots with error bars) and fits from ab initio (solid red lines) and rigid body models (dashed blue lines): curve 1, importin α/β complex (measured at 0.5 mg/mL); curve 2, NP/ΔIBB−importin α complex; curve 3, NP/α/β complex. (b) Pair distance distribution functions, with the same notations as in panel a.

structure in the denatured protein. By contrast, full-length importin α displays a more cooperative thermal transition. Binding to NP has a stabilizing effect on both ΔIBB−importin α (whose main transition T_m shifts from 34.0 to 41.5 °C) and importin α (shifting from 41.5 to 47 °C) (Figure 5a,b). It is important to note that NP, a hyperstable protein, does not suffer any transition in this temperature range (*33*, *67*). Stabilization of importin α upon association with NP is also observed to the same extent in the case of NP13D (data not shown). The increase in T_m associated with NLS recognition is smaller in the case of full-length importin α than ΔIBB−importin α: one should consider that in full-length importin α, the NLS binding site is occupied either by its autoinhibitory IBB domain (in the absence of NP) or by the NLS (in the complex with NP), while in ΔIBB−importin α, the NLS binding site changes from being empty and exposed to a covered state. In that sense, these data reflect the fact that binding to an authentic NLS is more stabilizing for importin α that binding to its own NLS-resembling IBB domain, and this might be due to the bipartite structure of the NLS (in contrast to the "monopartite" character of the IBB), which acts as a bivalent "staple" on the flexible importin α. It should also be noted that a relatively low affinity (4 μM) has been reported (*37*) for the binding of the IBB domain to ΔIBB−importin α (e.g., in trans), reflecting the fact that this interaction is less optimal than that of functional NLSs.

We observed that the binding of an NLS peptide to importin α results in the same stabilization (not shown) as the binding of full-length NP. This, in analogy to what is discussed for the binding of importin α to importin β, suggests that the two proteins are solely linked through the NLS segment.

In conclusion, these results indicate that binding to NP conformationally stabilizes importin α. Ligand-induced stabilization is a usually observed phenomenon and a symptom of bona fide specific interactions between proteins (*68*). Additionally, our data suggest that in the NP/α/β complex, the individual proteins behave as separate units that are solely connected by their respective ligand-binding motifs.

Small-Angle X-ray Scattering-Derived Solution Structure of the Importin α/β/NP Complex. The structural parameters of the proteins and complexes studied (Table 2) were determined from the experimental scattering patterns (Figure S3 of the Supporting Information and Figure 6). The values of the

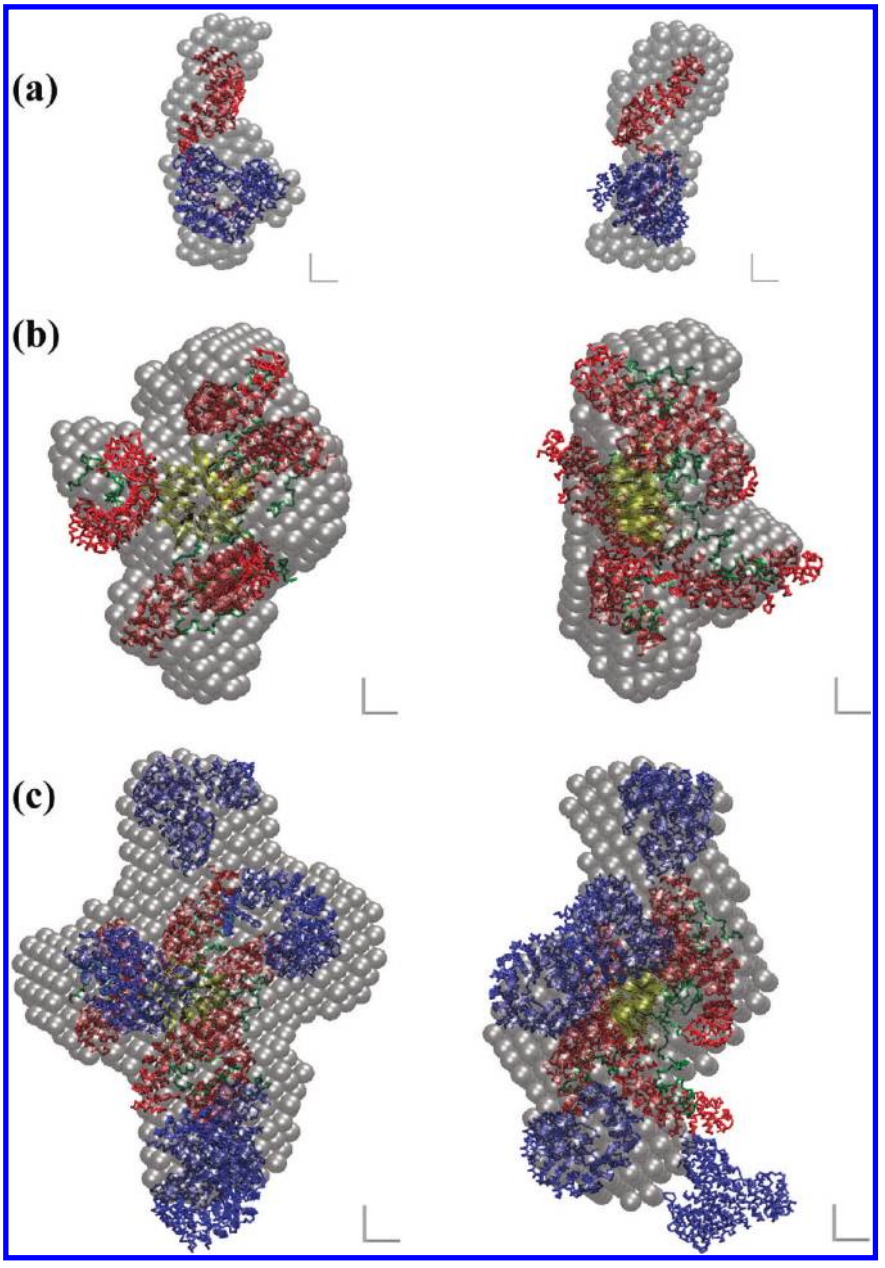

FIGURE 7: Structural models. Ab initio and rigid body models of the complexes. (a) Importin α/β complex (1:1 ratio). Ab initio model (gray beads) is superimposed with the rigid body model [C_α traces are red for the ARM domain region of importin α, purple for the IBB domain, and blue for importin β; the hypothetical position of the linker (C_α atoms) between the IBB and ARM domains is represented as red spheres]. (b) ΔIBB−importin α/NP complex (5:1 stoichiometry). An ab initio model (gray beads) is superimposed with the rigid body model in which the NP core domain (PDB entry 1K5J) is displayed as yellow ribbons and C-terminal tail domains of NP are indicated by green C_α traces, and five ΔIBB−importin α molecules (PDB entry 1EE5) are represented as red C_α traces. (c) Importin NP/α/β complex (1:5:5 stoichiometry). An ab initio model (gray beads) is superimposed with the rigid body model in which the NP core and tail domains and importin α are represented as in panel b, and five importin β molecules bound to the IBB domain (PDB entry 1QGK) are displayed as blue C_α traces. The right views are rotated counterclockwise around the vertical axis. The scale bars represent 2 nm.

radius of gyration (R_g) and the maximum dimension (D_{max}) of importin molecules point to an elongated shape. The values of the estimated apparent molecular weight (MW_{exp}) and hydrated particle volume (V_p) indicate that ΔIBB−importin α exists mainly as dimers at the concentrations used in SAXS (2−10 mg/mL) (Table 2). At lower concentrations (0.25−1 mg/mL), ΔIBB−importin α was found to be in a monomer−dimer equilibrium (data not shown) where the volume fraction of monomers is ~55−60% and the volume fraction of dimers is 40−45% as determined by OLIGOMER (*51*). Indeed, the ability of importin α to dimerize in solution has been documented (*69*). Because importin α and ΔIBB−importin α bind to NP as monomers (see below), the availability of the monomeric species is granted by the re-establishment of the monomer−dimer equilibrium.

By contrast, free importin β is monomeric in solution at all tested concentrations (Table 2), and in agreement with reported SAXS data (*26*), its scattering pattern points to an open conformation, unlike the Ran-bound (*28*) or IBB-bound (*22*) structures. The SAXS parameters of the importin α/β complex are found to depend also on the concentration: an importin α/β heterodimer is observed at a concentration of 0.5 mg/mL, while dimerization of heterodimers occurs at higher concentrations (2−10 mg/mL). Therefore, the model of the α/β heterodimer was constructed for a concentration of 0.5 mg/mL.

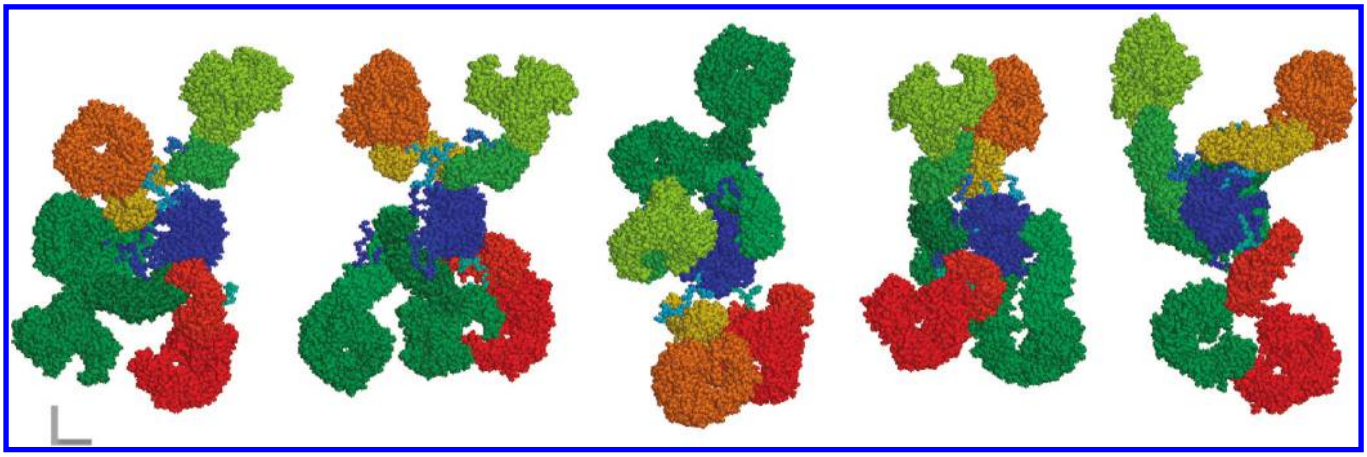

FIGURE 8: Flexibility of the NP/α/β complex. Different rigid body models of the importin NP/α/β complex obtained without symmetry confirm the high degree of flexibility for the orientations of importin α/β with respect to the NP core domain. The core domain is colored blue. The scale bars represent 2 nm.

The R_g and D_{max} values for ΔIBB−importin α and the importin α/β heterodimer in a complex with NP confirm binding of multiple importin molecules to NP. Furthermore, we were able to confirm the reliability of 5:1 and 5:5:1 complex stoichiometry for ΔIBB−importin α and importin α/β bound to NP, respectively. Indeed, the hydrated particle volume of the NP/α/β complex is equal to 1800 ± 100 nm^3, which nicely corresponds to the theoretical molecular weight (MW) of 900 kDa for the 1:5:5 stoichiometry. In the case of the NP/ΔIBB−importin α complex, the excluded volume is 810, also pointing to 1:5 stoichiometry.

The pair distance distributions [$p(r)$] computed from the experimental data are given in Figure 6b. The observed asymmetric tails are typical for extended molecules. The $p(r)$ function of the NP/α/β complex displays a maximum value further shifted toward larger distances, which is typical for particles that are not compact (*70*), as shown in the proposed models presented below.

The low-resolution shapes of the complexes under study (importin α/β, NP/ΔIBB−importin α, and NP/α/β) (Figure 7 and Figure S4 of the Supporting Information) were reconstructed ab initio with DAMMIF (*55*). Good fits to the scattering data (Figure 6a) were obtained with discrepancies ("χ") of 1.12, 1.06, and 1.24, respectively.

To construct more detailed models of the importin α/β complex, we used an approach that made use of the known high-resolution structures of ΔIBB−importin α (PDB entry 1EE5, without the NLS moiety) (*15*) and of importin β bound to IBB (PDB entry 1QGK) (*22*). The maximum distance between the ARM repeat region and the IBB domain and the relative orientation of the IBB motif with respect to the importin β molecules were imposed as restrictions. The positions and orientations of the subunits were restored by SASREF (*59*) (for details, see Experimental Procedures). The most typical selected rigid body heterodimer model that overlaps well with the ab initio model (Figure 7a) represents both proteins as two independent domains solely connected through the IBB domain.

For the model of the NP/ΔIBB−importin α complex, the BUNCH-restored fragments of C-terminal domains of full-length NP (residues 120−200 for each monomer) (*60*) were connected to the corresponding parts of the NP core pentamer and five ΔIBB−importin α molecules (PDB entry 1EE5) (*15*) were taken as rigid bodies. Alternative modeling using the crystal structure of mouse importin α in a complex with NLS (PDB entry 1EJY) (*16*) yielded practically the same result (not shown). Appropriate restrictions [maximum distance allowed between the NP core domain and NLS motif, antiparallel orientation of importin α and NLS, and the presence of the interacting residues between NLS segments of NP tail and the middle part of importin α (for details, see Experimental Procedures)] were taken into account for the modeling. In the refined model, which overlaps well with the ab initio model (Figure 7b), NP tails adopt a slightly asymmetric distribution around the NP core domain. ΔIBB−importin α molecules interact mainly with these tail domains of NP and protrude away from the NP core.

For modeling of the NP/α/β complex, either the high-resolution crystallographic structures of importin α and importin β [PDB entries 1EE5 (*15*) and 1QGK (*22*)] or the α/β heterodimer model previously built (Figure 7a) was used. Both approaches gave similar quality fits. In the representative rigid body model of the NP/α/β complex, shown in Figure 7c, importin α molecules interact with the C-terminal domains of NP protruding away from the NP core domain while importin β molecules, in turn, lie adjacent to importin α moieties. This complex further presents a more anisometric shape than the binary NP/ΔIBB−importin α complex. To accommodate five bulky heterodimers, NP tails are forced to change their relative orientation to avoid steric clashes.

Figure 7c shows that the average ab initio model overlaps well with the representative rigid body models, which indicates that the overall shape of the NP/α/β ternary complex can be reliably reconstructed from the SAXS data (see also further comparison of the most representative ab initio and rigid body models in Figure S4 of the Supporting Information). It must be noted, however, that for such a complicated assembly the rigid body modeling does not provide a unique solution. Indeed, different SASREF runs (from 20 total runs) provide models with varying organizations of domains within approximately the same elongated overall shape (Figure 8 displays five typical models fitting the data well with χ values between 1.24 and 1.37). Therefore, SASREF models may represent individual structures (states) that are present in a flexible complex. On the other hand, ab initio shape determination for such systems provides only an average model, which may contain some artificial features induced by flexibility. It might be tempting to speculate that these results point to the flexibility of the ternary complex in solution (which is quite conceivable given the presence of the flexible linkers in NP), but the observed variability could to some extent also be

caused by the inherent ambiguity of the interpretation of the SAXS data.

To further assess the possible flexibility of the NP/importin complexes, we have estimated their sizes by DLS. The hydrodynamic radii (R_h) of NP/ΔIBB−importin α and NP/α/β complexes were found to be 5.5 ± 0.2 and 6.8 ± 0.2 nm, respectively. These values are smaller than the radii of gyration (R_g) obtained from SAXS (Table 2), yielding R_g/R_h ratios of 1.17 and 1.26 for the NP/ΔIBB−importin α and NP/α/β complexes, respectively. The R_g/R_h ratio exceeding unity points to the presence of flexible fragments in a macromolecule or complex (*71*), and the higher the ratio, the higher the flexibility. Therefore, the NP/importin complexes, and especially the ternary complex, do display flexibility in solution.

To quantitatively characterize the flexibility of the ternary complex, we have used the ensemble optimization method (EOM). The obtained R_g distribution of the selected (optimized) models [which are similar to SASREF models and provide fits with a χ of 1.27 (see Figure S5 of the Supporting Information)] shows a skewed peak around 8−9 nm, confirming the noticeable flexibility of the complex. On the other hand, the selected ensembles display a much narrower R_g distribution than the randomly generated pool, and in particular, a complete absence of model R_g values exceeding 10 nm, which indicates that the structural flexibility is rather limited and only relatively compact models similar to those presented in Figure 7c are present in solution.

DISCUSSION

The importin α/β heterodimer mediates the "classical" nuclear transport pathway for the import of many proteins bearing a nuclear localization sequence (NLS), such as nucleoplasmin. The studies that have characterized the molecular interactions within this machinery have so far mostly focused on the recognition of small protein fragments (i.e., binding of importin α to the NLS motif and binding of importin β to the IBB domain of importin α). We have instead approached the formation of nativelike, entire complexes between the full-length proteins involved.

Formation of the complex between importin α and β is governed by a favorable enthalpy change, in agreement with the polar nature of the main interactions revealed by the crystal structure of the IBB/importin β complex, that shows electrostatic interactions between the inner surface of importin β, bearing mainly acidic residues, and the highly positively charged (+9 net charges) IBB domain (*22*). The similarity of the Δc_P estimated from the molecular surface area buried in this complex (*22*) with that experimentally determined by ITC, together with the thermal behavior of the α/β complex, which shows distinct transitions corresponding to the two proteins, suggests that importin α and importin β remain as independent units in the heterodimer, connected by only the IBB domain. This is confirmed by the SAXS solution structure of the α/β heterodimer, both alone and bound to NP: importin α and β do not present a compact, "intimate" interaction but instead behave as independent bodies.

The strong binding of importin α/β to NP (57 nM) nicely correlates with the previously reported affinity of ΔIBB−importin α and α/β for NLS peptides (*17*, *37*, *66*), although in vivo studies (*43*) have revealed a lower binding affinity because of the influence of the cellular environment. Also, it should be noted that, because of the differences in specificity between importin α subtypes (*65*), the in vivo affinity could depend on the particular importin isoform. The binding process that we observe is enthalpy-driven and counterbalanced by an unfavorable entropy change, indicating that hydrogen bond, van der Waals, and/or electrostatic interactions dominate the formation of the complex. This agrees with the crystal structures of truncated importin α bound to NLS peptides (*14*−*21*), reflecting that the interactions are mainly of polar character: (i) hydrogen bonds between importin-conserved Asn side chains and NLS main chain atoms, (ii) salt bridges between NLS basic residues and importin negatively charged amino acids, and (iii) polar interactions between those basic residues and the helix dipoles of the ARM repeat H3 helices. Nevertheless, there are also hydrophobic interactions between conserved Trp residues of importin and the aliphatic part of NLS Lys side chains (*14*, *16*). The entropic penalty associated with the binding most probably reflects an ordering effect on the otherwise flexible and mobile NLS motifs upon the interaction event.

We found that importin α/β binds to NP with a stoichiometry of five heterodimers per NP pentamer, proving that all five available binding sites of NP are occupied by importins. Whereas in vivo, binding of one α/β heterodimer to any protein should be enough to deliver it to the nucleus, it has been reported that the presence of multiple NLSs in NP (*34*) enhances its nuclear accumulation, suggesting that the number of NLSs might govern the traffic rate, which could be an advantage for oligomeric nuclear proteins.

The binding of importin α/β to full-length NP shows a heat capacity change similar to that of the NLS peptide, suggesting that the recognition is solely mediated by the NLS motif, which is further supported by the same extent of thermal stabilization upon binding to both NP and NLS (data not shown). That the NLS recognition is not significantly affected by the protein context is not surprising considering the flexibility of the NP tail domains (*33*), harboring the NLS segments.

We found that a chromatin remodeling active NP mutant that mimics phosphorylation of 13 residues, including those of the tail domain in the proximity of the NLS, displays the same importin binding properties as wild-type NP. Although this mutant is functionally most similar to natural authentically phosphorylated NP (*36*), the possibility remains that substitution of phosphorylatable residues for Asp does not reproduce the effect of real phosphorylation regarding the interaction with importin. However, it is interesting to note that Kobe et al. (*17*) did not find significant differences between the importin binding to an NLS peptide from a protein whose import is phosphorylation-regulated and the same peptide phosphorylated in several residues. Alternatively, if phosphorylation does regulate NP transport, it would affect some other aspect of the import route. It has been found that importin itself is phosphorylated at several residues (*72*). Several of them map near the NLS binding site, suggesting the intriguing possibility that they could influence the interaction with the cargo protein.

Small-angle X-ray scattering has been proven to be a suitable methodology for the study of flexible and multidomain systems (*71*, *73*). Given that our complexes are formed by multiple proteins that present flexible domains, this technique could provide valuable information about the transport machinery. We present the first 3D structural model of a complete nuclear transport complex with an oligomeric cargo. It shows how NP can accommodate five importin α/β heterodimers embracing the tail domains. The existence of multiple models that fit equally well the experimental SAXS data reflects the inherent flexibility of the particle and is given by the flexible linkers between the NP core domain and the

NLS (residues 121−154 of NP). Although, as a consequence of this flexibility, importin ligands can occasionally come into proximity between them and the NP core, the structure is consistent with the notion that the canonical binding elements (NLS and IBB) are the ones determining the molecular basis of the recognition.

We have recently presented structural models of NP bound to other ligands, histones H5 and H2AH2B, using SAXS (*60*). These complexes, which were modeled using *P*5 symmetry, have a much more compact shape than the NP/α/*β* complex, because histones (smaller in size than importins) interact with both the tail and core domains of NP. In the NP/α/*β* complex, however, the NLS motif is connected by a long (35 residues) and flexible linker to the core domain of NP; therefore, application of symmetry is not justified in this system. We did try to perform an alternative rigid body analysis of the binary and ternary NP/importin complexes assuming *P*5 symmetry, and the obtained models (not shown) yielded significantly worse fits compared to the *P*1 models presented above. Moreover, none of the selected models obtained with the ensemble optimization method show a symmetric shape. The SAXS data therefore also suggest that the *P*5 symmetry is absent (or possible only for the minority part of the species) for the NP/importin complexes.

The structural basis of importin recognition of not only NLS peptides but also entire protein domains has been documented for the C-terminal domain of the PB2 subunit from the influenza virus polymerase (*41*) and the CBP80 subunit of the cap binding complex (*42*). Both crystal structures show, in agreement with our conclusions, that the binding mode of the bipartite NLS segments is similar to what has been described for isolated NLS peptides (*15*, *16*). The study by Dias et al. (*42*) also provides a structural model obtained by SAXS of the complex formed by CBP80, importin α, and importin *β*. We have compared our structure of the NP-bound importin α/*β* with that described by Dias et al. (*42*), finding that the relative orientation of the two importins is very similar [superposition of the α/*β* heterodimer from both structures gives a normalized spatial discrepancy (NSD) of 1.5]. In analogy to their model (*42*), our structure of the NP/α/*β* complex shows that the three proteins behave as independent units and raises the possibility of variation in the relative orientation of the proteins, e.g., reflecting the inherent flexibility of the complex.

The saturated α/*β*/NP complex is a big particle: its maximum diameter is approximately 28 nm as estimated by SAXS (Table 2). This size should allow passage of the complex through the NPC, whose nominal effective diameter has been estimated to be 35−40 nm (*74*). Besides, the flexibility of its structure suggests that it might adopt a more compact conformation or "squeeze" if required to facilitate transit into the nucleus. Importin *β* is responsible for the passage of the transport complex through the NPC by virtue of its interactions with FG nucleoporins that fill the interior of the pore forming a meshlike matrix (*3*). Conformational flexibility of importin *β* has been widely discussed (*25*, *26*) and is important for its functional role. It is probable that the nature of the NPC interior determines the requirement of flexibility not only of the transporter (importin *β*) but also, in general, of the entire transport complex, which must permeate through the FG-rich meshwork. The multiple binding sites for importin in the NP oligomer could represent an advantage for transit: the presence of various importin *β* molecules connected by flexible linkers to the particle core could allow the cargo to "hold" to the NPC inside with alternatively stepping "feet", affording in this way a more effective (not slippery) translocation.

In conclusion, we have thermodynamically and structurally characterized the formation of the nuclear transport complex of importin α/*β* with the oligomeric protein nucleoplasmin. We have found that the NP pentamer can bind with high affinity five α/*β* heterodimers. The formed multidomain complex shows an extended shape and remains stable by virtue of two attachment points: recognition of the NLS by importin α and recognition of the IBB domain by importin *β*, which otherwise allow for conformational flexibility. This modular and articulated architecture might facilitate the passage of such a large particle through the nuclear pore complex.

ACKNOWLEDGMENT

We thank Dr. D. Görlich (Heidelberg, Germany) for his generous gift of importin clones, Dr. A. Muga (Bilbao, Spain) for helpful discussions, and Dr. Cerione for making the coordinates of their SAXS structural model available to us.

SUPPORTING INFORMATION AVAILABLE

A control ITC experiment with a NLS-defective NP mutant, CD spectra of NP and NP/importin complexes, SAXS data for ΔIBB−importin α, the α/*β* (2:2) complex, and importin *β*, and ensemble optimization method results. This material is available free of charge via the Internet at http://pubs.acs.org.

REFERENCES

1. Görlich, D., and Kutay, U. (1999) Transport between the cell nucleus and the cytoplasm. *Annu. Rev. Cell Dev. Biol. 15*, 607–660.
2. Pemberton, L. F., and Paschal, B. M. (2005) Mechanisms of receptor-mediated nuclear import and nuclear export. *Traffic 6*, 187–198.
3. Stewart, M. (2007) Molecular mechanism of the nuclear protein import cycle. *Nat. Rev. Mol. Cell Biol. 8*, 195–208.
4. Goldfarb, D. S., Corbett, A. H., Mason, D. A., Harreman, M. T., and Adam, S. A. (2004) Importin α: A multipurpose nuclear-transport receptor. *Trends Cell Biol. 14*, 505–514.
5. Dingwall, C., and Laskey, R. A. (1991) Nuclear targeting sequences: A consensus? *Trends Biochem. Sci. 16*, 478–481.
6. Lange, A., Mills, R. E., Lange, C. J., Stewart, M., Devine, S. E., and Corbett, A. H. (2007) Classical nuclear localization signals: Definition, function, and interaction with importin α. *J. Biol. Chem. 282*, 5101–5105.
7. Radu, A., Blobel, G., and Moore, M. S. (1995) Identification of a protein complex that is required for nuclear protein import and mediates docking of import substrate to distinct nucleoporins. *Proc. Natl. Acad. Sci. U.S.A. 92*, 1769–1773.
8. Rexach, M., and Blobel, G. (1995) Protein import into nuclei: Association and dissociation reactions involving transport substrate, transport factors, and nucleoporins. *Cell 83*, 683–692.
9. Izaurralde, E., Kutay, U., von Kobbe, C., Mattaj, I. W., and Görlich, D. (1997) The asymmetric distribution of the constituents of the Ran system is essential for transport into and out of the nucleus. *EMBO J. 16*, 6535–6547.
10. Peifer, M., Berg, S., and Reynolds, A. B. (1994) A repeating amino acid motif shared by proteins with diverse cellular roles. *Cell 76*, 789–791.
11. Kobe, B. (1999) Autoinhibition by an internal nuclear localization signal revealed by the crystal structure of mammalian importin α. *Nat. Struct. Biol. 6*, 388–397.
12. Görlich, D., Henklein, P., Laskey, R. A., and Hartmann, E. (1996) A 41 amino acid motif in importin-α confers binding to importin-*β* and hence transit into the nucleus. *EMBO J. 15*, 1810–1817.
13. Weis, K., Ryder, U., and Lamond, A. I. (1996) The conserved amino-terminal domain of hSRP1 α is essential for nuclear protein import. *EMBO J. 15*, 1818–1825.
14. Conti, E., Uy, M., Leighton, L., Blobel, G., and Kuriyan, J. (1998) Crystallographic analysis of the recognition of a nuclear localization signal by the nuclear import factor karyopherin α. *Cell 94*, 193–204.
15. Conti, E., and Kuriyan, J. (2000) Crystallographic analysis of the specific yet versatile recognition of distinct nuclear localization signals by karyopherin α. *Structure 8*, 329–338.

16. Fontes, M. R., The, T., and Kobe, B. (2000) Structural basis of recognition of monopartite and bipartite nuclear localization sequences by mammalian importin-α. *J. Mol. Biol. 297*, 1183–1194.
17. Fontes, M. R., The, T., Toth, G., John, A., Pavo, I., Jans, D. A., and Kobe, B. (2003) Role of flanking sequences and phosphorylation in the recognition of the simian-virus-40 large T-antigen nuclear localization sequences by importin-α. *Biochem. J. 375*, 339–349.
18. Chen, M.-H., Ben-Efraim, I., Mitrousis, G., Walker-Kopp, N., Sims, P. J., and Cingolani, G. (2005) Phospholipid scramblase 1 contains a nonclassical nuclear localization signal with unique binding site in importin-α. *J. Biol. Chem. 280*, 10599–10606.
19. Cutress, M. L., Whitaker, H. C., Mills, I. G., Stewart, M., and Neal, D. E. (2008) Structural basis for the nuclear import of human androgen receptor. *J. Cell Sci. 121*, 957–968.
20. Yang, S. N. Y., Takeda, A. A. S., Fontes, M. R. M., Harris, J. M., Jans, D. A., and Kobe, B. (2010) Probing the specificity of binding to the major nuclear localization sequence-binding site of importin-α using oriented peptide library screening. *J. Biol. Chem. 285*, 19935–19946.
21. Giesecke, A., and Stewart, M. (2010) Novel binding of the mitotic regulator TPX-2 (Target protein for *Xenopus* kinesin-like protein 2) to importin-α. *J. Biol. Chem. 285*, 17628–17635.
22. Cingolani, G., Petosa, C., Weis, K., and Muller, C. W. (1999) Structure of importin-β bound to the IBB domain of importin-α. *Nature 399*, 221–229.
23. Lee, S. J., Matsuura, Y., Liu, S. M., and Stewart, M. (2005) Structural basis for nuclear import complex dissociation by RanGTP. *Nature 435*, 693–696.
24. Liu, S. M., and Stewart, M. (2005) Structural basis for the high-affinity binding of nucleoporin Nup1p to the *Saccharomyces cerevisiae* importin-β homologue, Kap95p. *J. Mol. Biol. 349*, 515–525.
25. Conti, E., Muller, C. W., and Stewart, M. (2006) Karyopherin flexibility in nucleocytoplasmic transport. *Curr. Opin. Struct. Biol. 16*, 237–244.
26. Fukuhara, N., Fernández, E., Ebert, J., Conti, E., and Svergun, D. (2004) Conformational variability of nucleo-cytoplasmic transport factors. *J. Biol. Chem. 279*, 2176–2181.
27. Lee, S. J., Imamoto, N., Sakai, H., Nakagawa, A., Kose, S., Koike, M., Yamamoto, M., Kumasaka, T., Yoneda, Y., and Tsukihara, T. (2000) The adoption of a twisted structure of importin-β is essential for the protein-protein interaction required for nuclear transport. *J. Mol. Biol. 302*, 251–264.
28. Vetter, I. R., Arndt, A., Kutay, U., Görlich, D., and Wittinghofer, A. (1999) Structural view of the Ran-Importin β interaction at 2.3 Å resolution. *Cell 97*, 635–646.
29. Frehlick, L. J., Eirín-López, J. M., and Ausió, J. (2007) New insights into the nucleophosmin/nucleoplasmin family of nuclear chaperones. *BioEssays 29*, 49–59.
30. Prado, A., Ramos, I., Frehlick, L. J., Muga, A., and Ausió, J. (2004) Nucleoplasmin: A nuclear chaperone. *Biochem. Cell Biol. 82*, 437–445.
31. Akey, C. W., and Luger, K. (2003) Histone chaperones and nucleosome assembly. *Curr. Opin. Struct. Biol. 13*, 6–14.
32. Dutta, S., Akey, I. V., Dingwall, C., Hartman, K. L., Laue, T., Nolte, R. T., Head, J. F., and Akey, C. W. (2001) The crystal structure of nucleoplasmin-core: Implications for histone binding and nucleosome assembly. *Mol. Cell 8*, 841–853.
33. Hierro, A., Arizmendi, J. M., De Las Rivas, J., Urbaneja, M. A., Prado, A., and Muga, A. (2001) Structural and functional properties of *Escherichia coli*-derived nucleoplasmin. A comparative study of recombinant and natural proteins. *Eur. J. Biochem. 268*, 1739–1748.
34. Dingwall, C., Dilworth, S. M., Black, S. J., Kearsey, S. E., Cox, L. S., and Laskey, R. A. (1987) Nucleoplasmin cDNA sequence reveals polyglutamic acid tracts and a cluster of sequences homologous to putative nuclear localization signals. *EMBO J. 6*, 69–74.
35. Leno, G. H., Mills, A. D., Philpott, A., and Laskey, R. A. (1996) Hyperphosphorylation of nucleoplasmin facilitates *Xenopus* sperm decondensation at fertilization. *J. Biol. Chem. 271*, 7253–7256.
36. Bañuelos, S., Omaetxebarria, M. J., Ramos, I., Larsen, M. R., Arregi, I., Jensen, O. N., Arizmendi, J. M., Prado, A., and Muga, A. (2007) Phosphorylation of both nucleoplasmin domains is required for activation of its chromatin decondensation activity. *J. Biol. Chem. 282*, 21213–21221.
37. Catimel, B., The, T., Fontes, M. R., Jennings, I. G., Jans, D. A., Howlett, G. J., Nice, E. C., and Kobe, B. (2001) Biophysical characterization of interactions involving importin-α during nuclear import. *J. Biol. Chem. 276*, 34189–34198.
38. Harreman, M. T., Kline, T. M., Milford, H. G., Harben, M. B., Hodel, A. E., and Corbett, A. H. (2004) Regulation of nuclear import by phosphorylation adjacent to nuclear localization signals. *J. Biol. Chem. 279*, 20613–20621.
39. Hodel, M. R., Corbett, A. H., and Hodel, A. E. (2001) Dissection of a nuclear localization signal. *J. Biol. Chem. 276*, 1317–1325.
40. Cingolani, G., Lashuel, H. A., Gerace, L., and Muller, C. W. (2000) Nuclear import factors importin α and importin β undergo mutually induced conformational changes upon association. *FEBS Lett. 484*, 291–298.
41. Tarendeau, F., Boudet, J., Guilligay, D., Mas, P. J., Bougault, C. M., Boulo, S., Baudin, F., Ruigrok, R. W., Daigle, N., Ellenberg, J., Cusack, S., Simorre, J. P., and Hart, D. J. (2007) Structure and nuclear import function of the C-terminal domain of influenza virus polymerase PB2 subunit. *Nat. Struct. Mol. Biol. 14*, 229–233.
42. Dias, S. M., Wilson, K. F., Rojas, K. S., Ambrosio, A. L., and Cerione, R. A. (2009) The molecular basis for the regulation of the cap-binding complex by the importins. *Nat. Struct. Mol. Biol. 16*, 930–937.
43. Cardarelli, F., Bizzarri, R., Serresi, M., Albertazzi, L., and Beltram, F. (2009) Probing nuclear localization signal-importin α binding equilibria in living cells. *J. Biol. Chem. 284*, 36638–36646.
44. Poon, I. K., and Jans, D. A. (2005) Regulation of nuclear transport: Central role in development and transformation? *Traffic 6*, 173–186.
45. Vancurova, I., Paine, T. M., Lou, W., and Paine, P. L. (1995) Nucleoplasmin associates with and is phosphorylated by casein kinase II. *J. Cell Sci. 108* (Part 2), 779–787.
46. Sturtevant, J. M. (1977) Heat capacity and entropy changes in processes involving proteins. *Proc. Natl. Acad. Sci. U.S.A. 74*, 2236–2240.
47. Baldwin, R. L. (1986) Temperature dependence of the hydrophobic interaction in protein folding. *Proc. Natl. Acad. Sci. U.S.A. 83*, 8069–8072.
48. Murphy, K. P., and Freire, E. (1992) Thermodynamics of structural stability and cooperative folding behavior in proteins. *Adv. Protein Chem. 43*, 313–361.
49. Luque, I., and Freire, E. (1998) Structure-based prediction of binding affinities and molecular design of peptide ligands. *Methods Enzymol. 295*, 100–127.
50. Knaapila, M., Svensson, C., Barauskas, J., Zackrisson, M., Nielsen, S. S., Toft, K. N., Vestergaard, B., Arleth, L., Olsson, U., Pedersen, J. S., and Cerenius, Y. (2009) A new small-angle X-ray scattering set-up on the crystallography beamline I711 at MAX-lab. *J. Synchrotron Radiat. 16*, 498–504.
51. Konarev, P. V., Volkov, V. V., Sokolova, A. V., Koch, M. H. J., and Svergun, D. I. (2003) PRIMUS: A Windows-PC based system for small-angle scattering data analysis. *J. Appl. Crystallogr. 36*, 1277–1282.
52. Guinier, A. (1939) La diffraction des rayous X aux tres petits angles: application a l'etude de phenomenes ultramicroscopiques. *Ann. Phys. 12*, 161–237.
53. Svergun, D. I. (1992) Determination of the regularization parameter in indirect transform method using perceptual criteria. *J. Appl. Crystallogr. 25*, 495–503.
54. Porod, G. (1982) General theory. In Small-angle X-ray scattering (Glatter, O., and Kratky, O., Eds.) pp 17−51, Academic Press, London.
55. Franke, D., and Svergun, D. I. (2009) DAMMIF, a program for rapid ab-initio shape determination in small-angle scattering. *J. Appl. Crystallogr. 42*, 342–346.
56. Svergun, D. I. (1999) Restoring low resolution structure of biological macromolecules from solution scattering using simulated annealing. *Biophys. J. 76*, 2879–2886.
57. Volkov, V. V., and Svergun, D. I. (2003) Uniqueness of ab initio shape determination in small angle scattering. *J. Appl. Crystallogr. 36*, 860–864.
58. Kozin, M. B., and Svergun, D. I. (2001) Automated matching of high- and low- resolution structural models. *J. Appl. Crystallogr. 34*, 33–41.
59. Petoukhov, M. V., and Svergun, D. I. (2005) Global rigid body modelling of macromolecular complexes against small-angle scattering data. *Biophys. J. 89*, 1237–1250.
60. Taneva, S. G., Bañuelos, S., Falces, J., Arregi, I., Muga, A., Konarev, P. V., Svergun, D. I., Velázquez-Campoy, A., and Urbaneja, M. A. (2009) A mechanism for histone chaperoning activity of nucleoplasmin: Thermodynamic and structural models. *J. Mol. Biol. 393*, 448–463.
61. Svergun, D. I., Barberato, C., and Koch, M. H. J. (1995) CRYSOL: A program to evaluate X-ray solution scattering of biological macromolecules from atomic coordinates. *J. Appl. Crystallogr. 28*, 768–773.
62. Bernadó, P., Mylonas, E., Petoukhov, M. V., Blackledge, M., and Svergun, D. I. (2007) Structural characterization of flexible proteins using small-angle X-ray scattering. *J. Am. Chem. Soc. 129*, 5656–5664.

63. Imamoto, N., Shimamoto, T., Kose, S., Takao, T., Tachibana, T., Matsubae, M., Sekimoto, T., Shimonishi, Y., and Yoneda, Y. (1995) The nuclear pore-targeting complex binds to nuclear pores after association with a karyophile. *FEBS Lett. 368*, 415–419.
64. Gascard, P., Nunomura, W., Lee, G., Walensky, L. D., Krauss, S. W., Takakuwa, Y., Chasis, J. A., Mohandas, N., and Conboy, J. G. (1999) Deciphering the nuclear import pathway for the cytoskeletal red cell protein 4.1R. *Mol. Biol. Cell 10*, 1783–1798.
65. Friedrich, B., Quensel, C., Sommer, T., Hartmann, E., and Köhler, M. (2006) Nuclear localization signal and protein context both mediate importin α specificity of nuclear import substrates. *Mol. Cell. Biol. 26*, 8697–8709.
66. Harreman, M. T., Hodel, M. R., Fanara, P., Hodel, A. E., and Corbett, A. H. (2003) The auto-inhibitory function of importin α is essential in vivo. *J. Biol. Chem. 278*, 5854–5863.
67. Taneva, S. G., Muñoz, I. G., Franco, G., Falces, J., Arregi, I., Muga, A., Montoya, G., Urbaneja, M. A., and Bañuelos, S. (2008) Activation of nucleoplasmin, an oligomeric histone chaperone, challenges its stability. *Biochemistry 47*, 13897–13906.
68. García-Álvarez, B., Bobkov, A., Sonnenberg, A., and de Pereda, J. M. (2003) Structural and functional analysis of the actin binding domain of plectin suggests alternative mechanisms for binding to F-actin and integrin *β*4. *Structure 11*, 615–625.
69. Percipalle, P., Butler, P. J., Finch, J. T., Jans, D. A., and Rhodes, D. (1999) Nuclear localization signal recognition causes release of importin-α from aggregates in the cytosol. *J. Mol. Biol. 292*, 263–273.
70. Koch, M. H., Vachette, P., and Svergun, D. I. (2003) Small-angle scattering: A view on the properties, structures and structural changes of biological macromolecules in solution. *Q. Rev. Biophys. 36*, 147–227.
71. Shiozawa, K., Konarev, P. V., Neufeld, C., Wilmanns, M., and Svergun, D. I. (2009) Solution structure of human Pex5.Pex14.PTS1 protein complexes obtained by small angle X-ray scattering. *J. Biol. Chem. 284*, 25334–25342.
72. Hachet, V., Kocher, T., Wilm, M., and Mattaj, I. W. (2004) Importin α associates with membranes and participates in nuclear envelope assembly in vitro. *EMBO J. 23*, 1526–1535.
73. von Ossowski, I., Eaton, J. T., Czjzek, M., Perkins, S. J., Frandsen, T. P., Schulein, M., Panine, P., Henrissat, B., and Receveur-Brechot, V. (2005) Protein disorder: Conformational distribution of the flexible linker in a chimeric double cellulose. *Biophys. J. 88*, 2823–2832.
74. Pante, N., and Kann, M. (2002) Nuclear pore complex is able to transport macromolecules with diameters of about 39 nm. *Mol. Biol. Cell 13*, 425–434.